Surface & Coatings Technology 266 (2015) 57–63

Contents lists available at ScienceDirect

Surface & Coatings Technology

journal homepage: www.elsevier.com/locate/surfcoat

Oxidation behavior of pack-cemented Si–B oxidation protection coatings for Mo–Si–B alloys at 1300 °C

Annika Lange [a,*,1], Martin Heilmaier [b], Travis A. Sossamann [c], John H. Perepezko [c]

[a] German Aerospace Center e. V. (DLR), Institute of Materials Research, Linder Hoehe, 51147 Cologne, Germany
[b] Karlsruhe Institute of Technology (KIT), Faculty of Mechanical Engineering, Engelbert-Arnold-Strasse 4, 76128 Karlsruhe, Germany
[c] University of Wisconsin—Madison, Department of Materials Science and Engineering, 1509 University Avenue, Madison, WI 53706, USA

ARTICLE INFO

Article history:
Received 1 December 2014
Accepted in revised form 6 February 2015
Available online 17 February 2015

Keywords:
Pack cementation
Oxidation protection coatings
Mo–9Si–8B

ABSTRACT

To enhance the resistance to oxidation and prolong the lifetime, oxidation protection coatings were applied on Mo–9Si–8B (in at.%) alloy substrates by Si–B co-pack cementation. Subsequently, the samples were conditioned at 1450 °C for 8 h in air to develop an outer 10 μm thick aluminoborosilicate scale. A multilayered microstructure of $MoSi_2$, Mo_5Si_3, and Mo_5SiB_2/MoB of about 80 μm thick was observed underneath the scale. During cyclic testing between room temperature and 1300 °C the samples exhibited a very low mass change of only up to $+/-0.2$ mg/cm^2 within 500 h at high temperature. During oxidation the $MoSi_2$ phase layer was partially consumed by silica and Mo_5Si_3 formation. No high material regression due to MoO_3-evaporation took place during testing. However, a low mass loss during the first 100 h of testing was observed, presumably due to stress cracking caused by thermal mismatch of coating and substrate accompanied by subsequent healing. The stresses were reduced by the growth texture in the [001] direction of the Mo_5Si_3-phase. In comparison to the uncoated substrate material, the mass change was decreased by 99.8%. This points to a significantly prolonged lifetime and shows the huge potential of coated Mo–9Si–8B alloys for application at very high temperatures and under thermal cycling loads.

1. Introduction

One way to improve the efficiency of gas turbines is to increase the turbine inlet temperature [1,2]. Current engines are limited by the temperature capability of the materials used in the first stages of the high pressure turbine. In fact, Ni-based superalloy blades equipped with internal cooling and coatings consisting of a thermal barrier layer and a bond coat show remarkable performance with lifetimes of more than 10,000 h and base metal temperatures of more than 85% of its melting temperature [3] but, a further increase in operating temperature with this system is unlikely due to the natural barrier of the melting temperature of Ni-base superalloys.

An alternative turbine blade material with a significantly higher melting point of more than 2000 °C is an Mo–Si–B based alloy, for example Mo–9Si–8B (at.%). The mechanical properties like creep and fatigue resistance are promising; however, their low ductility and oxidation behavior are still challenging [4–9]. For the latter, alloying with Zr and rare earth elements improves the oxidation behavior by reducing the mass loss due to MoO_3 evaporation and the adherence of the borosilicate scale [10,11]. Further improvement was shown by Mo, Si and B containing coatings applied by physical (PVD) or chemical vapor deposition (CVD) techniques [12–20].

One type of PVD oxidation protection layers was deposited by magnetron sputtering and was 5 μm thick [19]. Three-phase coatings consisting of Mo_5Si_3, $MoSi_2$ and MoB as well as $MoSi_2$ and MoB coatings with ratios of B/Si = 0.2 and 0.6 were analyzed. During oxidation treatment at 800, 1000 and 1300 °C a borosilicate layer was formed on the outer surface and was protective at 800 °C and 1000 °C for 100 h. At 1300 °C, the coated samples exhibited a significantly lower mass loss in comparison with the uncoated substrate; however, the lifetime of the thin coatings was limited. Beside oxidation, the $MoSi_2$–MoB coatings also degraded rapidly by interdiffusion with the substrate; therefore, 2 μm thick diffusion hindering layers were also applied by magnetron sputtering [20]. The coating lifetime was extended and mass loss of coated samples was reduced by this double layer setup. The diffusion hindering phase was Mo_5SiB_2 (T2), which is known to have this property due to its high atomic packing density. The procedure was proposed after analysis of CVD coatings [15,21,22].

The CVD coatings produced by co-pack cementation of Si and B exhibit an outer layer of about 20 μm $MoSi_2$ with MoB underneath [15]. Thus, previously described PVD coatings are similar to them. During oxidation treatment interdiffusion with the Mo-rich substrates takes place. Under the $MoSi_2$-layer a boron-saturated, oxidation stable Mo_5Si_3 layer and a MoB/Mo_5SiB_2 layer which hinders further diffusion

* Corresponding author.
E-mail address: lange.annika@gmx.de (A. Lange).
[1] Tel.: +49 2203 601 3512; fax: +49 2203 696480.

http://dx.doi.org/10.1016/j.surfcoat.2015.02.015
0257-8972/

and stabilizes the $MoSi_2$-rich coating were observed. On the sample surface an outer borosilicate layer forms which protects the substrate from further oxidation up to 1650 °C. On some samples, an aluminoborosilicate layer with Al stemming from the pack powder was also found [12,13,16,17]. This layer possesses a high resistance to calcia–magnesia–alumina–silica (CMAS). The pack cementation CVD coated samples show excellent oxidation behavior also on different materials like refractory alloys and SiC/C composites [12,13,17].

In this study the pack cemented coatings were deposited on a commercial Mo–9Si–8B alloy and cyclically tested at the aimed service temperature of 1300 °C [15,23]. The oxidation condition was already applied on Mo–9Si–8B alloy samples with magnetron sputtered oxidation protection coatings [19,20]. Consequently, the protectiveness and oxide scale formation of the CVD and PVD coatings can be compared directly. The focus of this paper is on this particular comparison as well as the coating morphology and development during testing of the CVD coatings on Mo–9Si–8B samples.

2. Materials and methods

The material with the nominal composition of Mo–9Si–8B–$0.2Y_2O_3$ (all numbers given in at.%) was produced by a powder metallurgical production route at Plansee SE, Reutte, Austria [5]. The microstructure consisted of about 50 vol.% Mo_{ss} (molybdenum solid solution) and the two intermetallic phases Mo_3Si (A15) and Mo_5SiB_2 (T2). Due to the oxygen content of 2000 ppm after mechanical alloying, some SiO_2 inclusions were also present in the microstructure after consolidation. Rectangular samples with a size of $15 \times 10 \times 1$ mm^3 were machined by spark erosion.

Prior to coating the samples were ground with SiC emery paper up to 2500 grit. The samples were coated by pack cementation, a CVD process which promotes diffusion via gaseous transport of Si and B into the Mo–9Si–8B alloy substrate by a halide activator. A powder mixture with a Si:B ratio of 35:1 was prepared, and composed of 34.03 wt.% Si (99.95% purity, 45 μm, Alfa Aesar), 0.97 wt.% B (99.95% purity, 45 μm, Alfa Aesar), 2.5 wt.% NaF activator (Alfa Aesar), and 62.5 wt.% Al_2O_3 spacer (180 μm). Samples were buried and gently compressed to achieve an intimate contact with approximately 10 g of powder mixture in an alumina crucible. The alumina crucible was sealed in an alumina tube, evacuated of air and purged with Ar gas (99.9% purity). The tube was placed in a furnace set to 1000 °C and run for 50 h under mild Ar flow.

The samples were conditioned partially at 1450 °C for 8 h in air before testing. During conditioning the coated sample is annealed in ambient air, which performs two essential roles. First, the annealing of the coating promotes the partial solid state transformation of $MoSi_2$ and MoB into the Mo_5Si_3 and Mo_5SiB_2 phases. This transformation acts to reduce thermal stresses between the coating and substrate, and provides a diffusion barrier to limit further penetration of silicon into the substrate. Secondly, the high temperature reaction air allows the coating to generate a uniform aluminoborosilica layer on the surface of the sample that resists further oxidation. Previous experience has shown that the conditioning procedure performed at temperatures ranging from 1400 to 1600 °C for times ranging from 10 to 2 h would result in sufficient phase transformation and aluminoborosilica formation to yield a coating structure with effective oxidation resistance [15].

The oxidation tests were performed in a laboratory muffle furnace at 1300 °C. The samples, supported by either an alumina crucible or SiC foam (Fig. 1), were placed in the 800 °C hot muffle furnace (Linn High Therm GmbH, Eschenfeld, Germany), which was heated at 12 K/min to 1300 °C. After a 10 h dwell time the furnace cooled slowly down in heat exchange with the environment. The samples were optically examined and weighed between each cycle. In total 10 or 50 cycles were performed equal to 100 or 500 h at 1300 °C. The first experiments were done in the alumina crucible, because the previous experiments with PVD-coatings performed at DLR were done in this way. During analysis of the CVD-coatings the origin of aluminum was not clear; therefore, the following experiments were done on the SiC foam to make sure that the aluminum is stemming from the pack and not the experimental setup.

The tested samples and one after conditioning were further examined by scanning electron microscopy (SEM) equipped with an energy dispersive X-ray spectroscopy detector (EDS). Micrographs were taken from the sample surface as well as from the cross section after metallographic preparation. A secondary electron (SE) detector and 5 kV acceleration voltage were used to chemically analyze the oxide scale. Micrographs of the coating were taken with a back scattered electron detector (BSE) using 15 kV. The crystalline phases were analyzed by X-ray diffraction (XRD) using Cu-K_α-radiation at 40 kV corresponding to a power of 1600 W. More information on equipment used is given in [20]. Furthermore, the crystallographic orientation of single phases and the distribution of the different phases within the coating were measured by electron backscatter diffraction (EBSD). A camera type Nordlys of Oxford Instruments was used with an acceleration voltage of 30 kV. The data was analyzed with the Channel 5 software.

3. Results

3.1. Mass change analysis after oxidation experiments

Fig. 2 depicts the normalized mass change during the 500 h of oxidation testing at 1300 °C. The two samples placed in the alumina crucible are indicated with filled symbols, and the two samples that were put on alumina-free SiC foam are symbolized with empty marks. All four samples suffered from material loss during the first 100 to 120 h of testing. After 100 h of oxidation exposure one sample of each condition was analyzed in the SEM. The remaining two samples were tested for an additional 400 h of exposure and experienced discontinuous mass gains. However, even though the time duration was too short to establish parabolic oxidation kinetics, the mass change is very low for testing at 1300 °C; with a maximum value of +/− 0.2 mg/cm^2. Even though the overall mass change is very small it appears in Fig. 2 that the mass change for the sample on SiC foam is greater than that for the sample

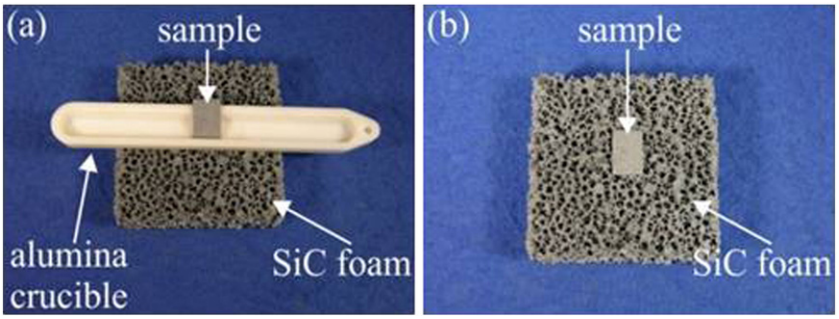

Fig. 1. Photograph of the coated Mo–Si–B samples (a) in the alumina crucible and (b) on the SiC foam.

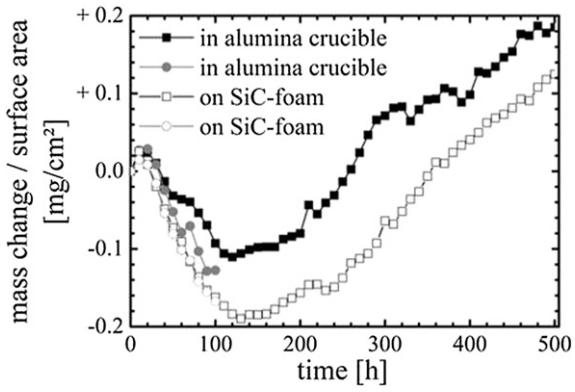

Fig. 2. Mass change per surface area versus time of the coated samples at 1300 °C.

on alumina. It is also evident that at early time the mass changes for both samples are identical. At about 100 h an offset of about 0.06–0.07 mg/cm^2 develops between the alumina and the SiC foam samples. For times greater than 100 h the rate of mass change (i.e. the slopes in Fig. 2) is identical for the two samples. Therefore, aside from the offset the mass change behavior is the same for the alumina and SiC foam sample. The offset could be caused by a handling loss for the SiC foam sample during weighing between cycles or due to a faster crack healing for the alumina sample, but the offset is very small. The analysis of the microstructural changes and the phase evolution elucidate the cause for the mass loss and deviation from parabolic behavior. It is assumed that the different sample holders do not have an effect on the mass change behavior because in the microstructure and chemical composition no difference was observed.

3.2. Coated Mo–9Si–8B sample in the as-packed and as-conditioned state

For comparison with the experiments a micrograph of the surface near areas of a sample in the as-packed state is shown in Fig. 3A. The outer layer is composed of $MoSi_2$ while the inner is MoB. No pores can be observed. Fig. 3B depicts the BSE-picture of the cross section of the Mo–9Si–8B alloy sample in the as-conditioned state. The sample is covered with an approximately 13 μm thick oxide scale. Underneath, a 46–54 μm thick $MoSi_2$ layer formed. Within this layer, bright Mo_5Si_3 inclusions and dark pores are present. The compositions were analyzed by EDS-analysis. Between the $MoSi_2$ layer and substrate the Si-content decreased to the substrate composition within a 22 μm thick interlayer. The median relation by EDS-analysis is Si/Mo = 0.6 which is consistent with the Mo_5Si_3-phase. Since the boron-content could not be analyzed with EDS, confirmation of the presence of the MoB and the Mo_5SiB_2 phases in this layer was not possible. However, according to the previous analyses of similar coatings on Mo-alloys it is likely that the two boron containing phases is formed between Mo_5Si_3 and substrate, as indicated in Fig. 3 [15]. The substrate contains many dark SiO_2-inclusions and pores. Both are stemming from the production of the substrate material. However, the higher pore density in the $MoSi_2$-rich region was caused by the conditioning treatment. The enrichment of the surface near sample areas with Si-rich phases causes a mismatch in thermal expansion of surface near regions and substrate (Table 1). This causes stresses which can result in cracks during cooling. Such cracks were observed in the $MoSi_2$- and Mo_5Si_3-rich layer, but were arrested by the Mo_5SiB_2 layer before propagating into the substrate.

Table 1
Coefficients of thermal expansion of Mo–9Si–8B substrate material and main coating phases $MoSi_2$, Mo_5Si_3(B) and Mo_5SiB_2.

Coefficient of thermal expansion	[100]-direction [$\cdot 10^{-6}$ K^{-1}]	[001]-direction [$\cdot 10^{-6}$ K^{-1}]
Substrate Mo–9Si–8B	5–6	5–6
$MoSi_2$ [30]	7.99	9.96
$Mo_5Si_{2,97}B_{0,16}$ [30]	5.72	13.9
Mo_5SiB_2 [31]	7.9	7.5

The oxide scale appears dark in the BSE-mode; therefore, SE-images were taken of this area. In the cross section (Fig. 4a) the oxide scale appears homogeneous besides some small bright inclusions in the lower region, which are presumably MoO_2. According to the EDS-analyses the composition of the oxide scale is 66O–27Si–5Al–2Na in at.%. The boron content could not be measured but is present according to other analysis of similar coatings [15]. Thus, the oxide scale is an aluminoborosilicate with Na-impurities stemming from the coating production. The top view of the sample (Fig. 4b) shows in addition randomly distributed bright inclusions in the oxide scale. Such inclusions are too small for an EDS-analysis and might be cristobalite (SiO_2), which is indicated by the faint peak in the XRD-pattern at about 22° or mullite ($3Al_2O_3 \cdot 2SiO_2$) which is indicated by the peak at about 26° in Fig. 5a.

The main structure of this scale is amorphous due to a high background between 20 and 30° in the 2 theta scan. The pattern also reveals the coating phases $MoSi_2$ and Mo_5Si_3, which formed in the outer regions. Molybdenum from the substrate and minor MoO_2-reflexes were also indicated. The intensity of the [002]- and [004]-reflections of the Mo_5Si_3-phase are higher than indicated in the database. This hints to a growth texture.

3.3. Coated Mo–9Si–8B sample after oxidation for 100 h

The cross sectional analyses of the samples placed on the SiC foam and in the Al_2O_3-crucible do not show significant differences in behavior after oxidation. Also, the Al-content in the oxide scales varies only between 3 at.%, which is rather attributed to variations in the powder pack than the different sample holders. Therefore, variations are not distinguishable between samples oxidized on the different holders.

The microstructure of the coating after oxidation for 100 h is depicted in Fig. 6a. In comparison to the sample in the as-conditioned state the density of pores increased. Also Si diffused further into the substrate during the high temperature treatment. As a result, the Mo_5Si_3-layer thickness grew to 40 μm. Additional bright Mo_5Si_3-regions in the

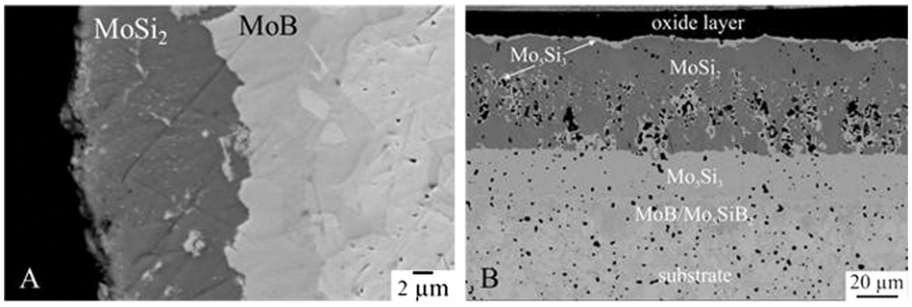

Fig. 3. BSE-picture of (A) the as-packed sample and (B) the conditioned coated Mo–9Si–8B sample.

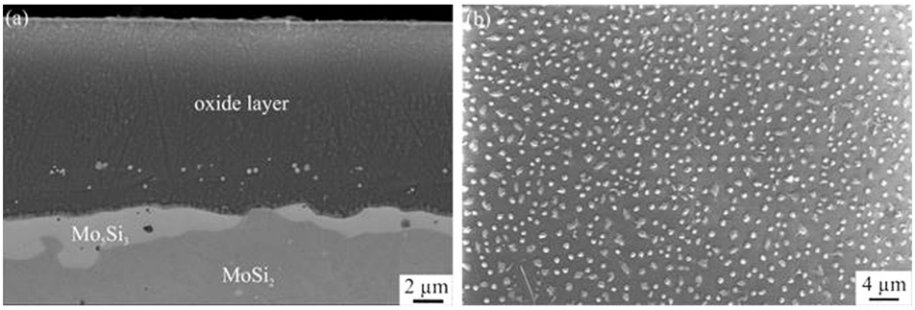

Fig. 4. SE-picture of the oxide scale of the as received sample (a) in cross-section and (b) top view.

$MoSi_2$-rich layer are present. This indicates Si-depletion on the surface near region either by oxide formation or interdiffusion. Due to the low increase of the oxide scale thickness, diffusion is the main reason. The thickness of the intermixed area of MoB/Mo_5SiB_2 could not be measured due to the low contrast in the BSE-image.

The microstructure of the oxide layer changed as well. Large needles grown in the glass layer were observed (Fig. 6b). The EDS-analysis of the coatings revealed 70O–5Al–25Si (+/−2 at.%). In comparison to the sample in the as-conditioned state, the scale was depleted of Na, probably due to volatilization. The needles are mullite-like crystals ($3Al_2O_3 \cdot 2SiO_2$), as indicated by the characteristic peaks in the XRD-pattern (Fig. 5b). Besides crystallization of mullite, more cristobalite is present due to the higher peak intensity at 22°.

To elucidate the coating microstructure in more detail EDS-mappings were performed (Fig. 7). The Al-content is localized in the oxide scale in discrete areas which hints to Al-rich mullite-like inclusions within the aluminoborosilicate scale. Also, apart from the SiO_2-inclusions in the substrate, oxygen was detected only in the outer oxide scale. This means that the coating is protective for at least 100 h of thermal cycling at 1300 °C. The mappings of Si and Mo show the $MoSi_2$ and Mo_5Si_3 regions, as well as the Si-lean interlayer of presumably MoB and Mo_5SiB_2 between Mo_5Si_3 and substrate.

The phase composition described above, especially the MoB/Mo_5SiB_2 interlayer, is confirmed by the EBSD-phase map in Fig. 8. In addition, some MoB inclusions underneath the $MoSi_2$ and within the Mo_5Si_3-layer are visible. Texture analyses (Fig. 9) showed that the Mo_5Si_3 phase grows preferentially with its [001] orientation (red color) oriented parallel to the y0-axis which is normal to the substrate surface.

3.4. Coated Mo–9Si–8B sample after oxidation for 500 h

After 500 h of oxidation at 1300 °C, equal to 50 cycles, almost all the $MoSi_2$ in the outer regions was decomposed (Fig. 10a) and Mo_5Si_3 is the main phase in the outer 135 µm of the sample. The Mo_5Si_3-layer under the porous region formerly composed of $MoSi_2$ grew from 40 µm to about 75 µm within the 400 h of oxidation at 1300 °C. A significant portion of the thickness increase derives from the phase conversion and associated volume change [15]. Despite these changes the MoB/Mo_5SiB_2-interlayer between substrate and Mo_5Si_3 is still present (Fig. 10b). This leads to saturation in boron of the Mo_5Si_3-phase which enhances the oxidation resistance of this phase. Therefore, the oxidation rate was not enhanced significantly because of the lack in oxidation resistant $MoSi_2$. Also, there was no further oxidation observed in the cracks. They also did not grow in depth. At higher magnification of the crack tip, pore agglomeration is present (Fig. 10c). Consequently, the coating is stable and protective until at least 500 h of thermal cycling at 1300 °C.

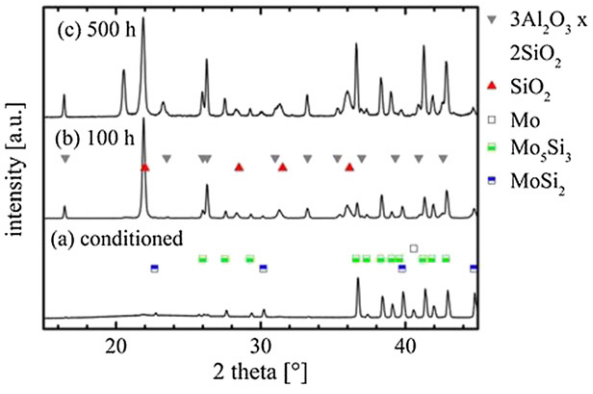

Fig. 5. XRD-pattern of the coated Mo–Si–B sample after (a) conditioning, oxidation for (b) 100 h and (c) 500 h.

4. Discussion

4.1. Mass change behavior of coated samples in contrast to bare substrate material

The improvement of oxidation resistance of the Mo–9Si–8B substrate samples coated with Si/B is remarkable. Previous oxidation studies with the bare substrate of the same alloy under the same oxidation treatment showed an initial mass loss of −66 mg/cm² [20]. After 100 h of testing the mass loss increased to −88 mg/cm². The comparison with the maximum mass loss of the coated samples after 100 h (−0.2 mg/cm²) indicates an improvement of 99.8% in terms of lower mass loss. This is equal to prolonged lifetime of any component based on Mo–9Si–8B alloys with coating, because the load bearing cross section of the intermetallic alloy is reduced much slower with a coating. Comparing the current results with those for the double layer PVD coating consisting of $MoSi_2$–MoB (B/Si = 0.2) and Mo_5SiB_2 layers, the mass loss of the PVD coating after 100 h at 1300 °C is −5.5 mg/cm² higher [20]. Thus, the oxidation resistance of CVD coatings is in this specific case higher and the lifetime longer due to an increased coating thickness. Moreover, it is useful to compare the performance of the Mo–Si–B based coating with that for other materials with silica or borosilica surface layers. For example, isothermal oxidation exposure for $MoSi_2$ at 1330 °C for 25 h results in a mass gain of 0.45 mg/cm² and the mass gain will increase with thermal cycling [24]. With single phase Mo_5SiB_2 isothermal oxidation at 1300 °C for 10 h yields a mass loss of 40 mg/cm² [25]. For the uncoated Mo–9Si–8B alloy exposure even at 1100 °C for 70 h results in a mass loss of about 23 mg/cm² [8]. This comparison indicates that the Mo–Si–B based coating design with a surface aluminoborosilica layer and an internal multiphase layering that exhibits thermodynamic stability and mechanical compatibility as well as an underlying diffusion barrier enables enhanced oxidation resistance over that for only silica or borosilica surface layers. For a detailed prediction of the lifetime the influence of the coating on the mechanical properties due to modification of the microstructure needs to be evaluated in the future.

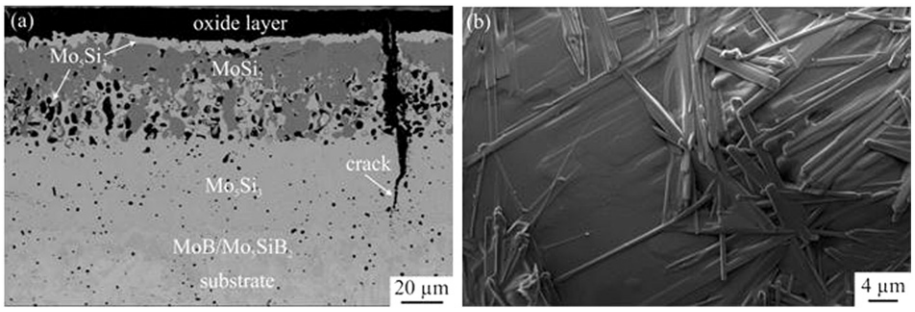

Fig. 6. (a) BSE-picture of the coated Mo–9Si–8B sample after oxidation at 1300 °C for 100 h (cross-sectional analysis) and (b) SE-picture of the oxide scale on this sample (top view).

4.2. Microstructure and interdiffusion of CVD coatings

The coating microstructure was already described in detail in previous publications and confirmed by these analyses [15]. During oxidation at 1300 °C the outer regions were depleted of Si by oxidation and by interdiffusion with the substrate, which can be observed by the increasing Mo_5Si_3(B)-layer thickness. This process was hindered by the MoB/Mo_5SiB_2-layer. The latter phase shows a low self-diffusion coefficient for Si [21]. The suitability of this phase was also already shown in a study in which a T2 interlayer was produced by PVD between an outer Si/B-rich oxidation protection layer and the Mo–9Si–8B substrate [20]. As shown in Fig. 9, the Mo_5Si_3 grew preferentially with its [001] crystal orientation normal to the substrate surface. We believe this to occur because this growth direction leads to a minimum mismatch of thermal expansion between coating and substrate. This may be rationalized as follows: The thermal expansion behavior of Mo_5Si_3(B) is known to be strongly anisotropic [30]. Table 1 summarizes the relevant coefficients of thermal expansion (CTE) with respect to the different crystal orientations. A growth of the Mo_5Si_3(B) phase with its [100] direction perpendicular to the surface would yield the [001]-direction with the large difference in CTE of $8–9 \cdot 10^{-6}\ K^{-1}$ to lie "in-plane" and, consequently, high stresses arising from thermal cycling. By contrast, interdiffusion of Si and the formation of Mo_5Si_3(B) with a [001] texture parallel to the substrate normal results in the [100]- and the [010]-directions to lie "in-plane" with the substrate surface. This leads to virtually zero thermal stresses due to the similarity between the CTEs of these two crystallographic directions ($5.72 \cdot 10^{-6}\ K^{-1}$) and that of the polycrystalline substrate being $5–6 \cdot 10^{-6}\ K^{-1}$. Thus, stresses seem to be highest after deposition and decrease during thermal treatment with growth of the Mo_5Si_3(B) layer. Therefore, any cracks present in the sample after 100 h of thermal cycling may have arrested upon further testing due to the loss in thermo-mechanical driving force.

4.3. Oxide scale formation and implication on mass loss

A change in chemical composition of the aluminoborosilicate scale during oxidation treatment was only observed in the Na content. Sodium was incorporated during pack cementation and evaporated during oxidation treatment. The incorporation and solution of alumina from the pack during coating synthesis account for the 3–6 at.% Al detected in the scale. An uptake from the alumina sample holder is unlikely because no differences in scale composition were observed between the two sample holders. In addition coatings produced by magnetron sputtering oxidized in the same alumina crucibles did not show any Al impurities [19,20].

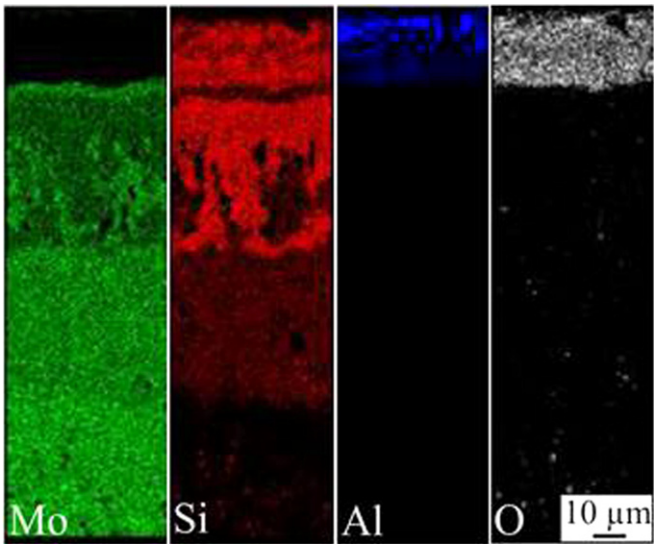

Fig. 7. EDS-mapping of the coated Mo–9Si–8B sample after oxidation at 1300 °C for 100 h.

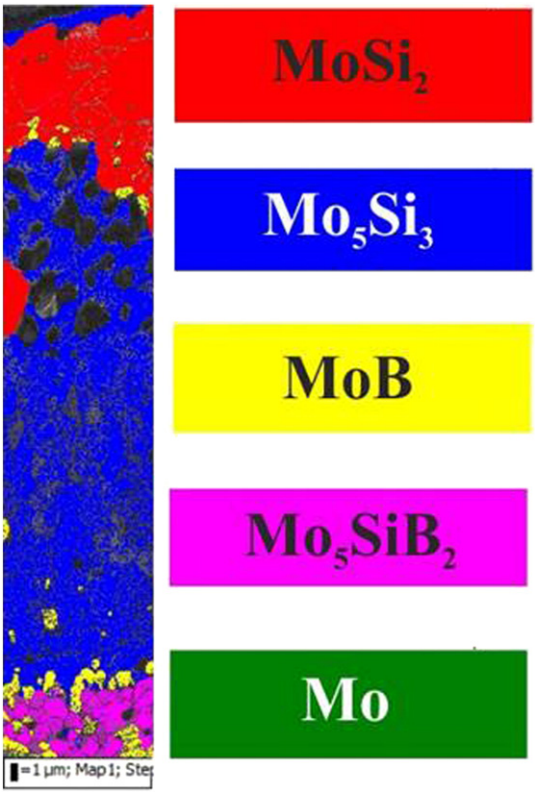

Fig. 8. EBSD mapping of the coated Mo–9Si–8B sample after oxidation at 1300 °C for 100 h.

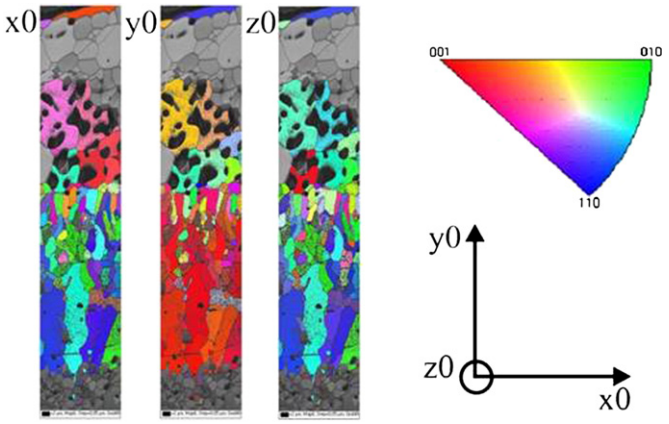

Fig. 9. IPF coloring of the Mo_5Si_3 phase with regard to the surface normal direction y0 in the coated Mo–9Si–8B sample after oxidation at 1300 °C for 100 h.

The aluminum in the aluminoborosilicate scale led to the formation of crystalline mullite. As indicated in Figs. 6 and 7 the crystalline needle morphology phases are confined to the top surface with the underlying aluminoborosilicate glass remaining. The crack formation due to stresses caused by thermal mismatch could have caused the mass loss within the first 100 h of oxidation during the initial period of heating with each cycle before the aluminoborosilicate becomes sufficiently fluid to heal the cracks. The reduced stresses accompanied with lower crack formation and growth might be the reason for the mass gain during the remaining 400 h of testing. The mass gain was caused by solid state transformation of $MoSi_2$ to Mo_5Si_3 with resulting formation of silica.

The differences beside the Al-impurities between the CVD and PVD coatings are the smaller pores and cracks in the PVD coating and the lower coating thickness. The latter cannot be increased easily due to the low sputtering rate. But with enhanced techniques such as high-power impulse magnetron sputtering (HiPIMS) [26,27] or gas flow sputtering [28,29] higher coating thicknesses could be deposited. By adjusting the coating parameters pores and cracks can also be avoided. Alloying elements which improve the coating performed and multilayered structures can also be applied directly. Nevertheless, such processes are expensive in comparison to pack cementation.

5. Conclusion

The main conclusions are the following:

1. In comparison to the uncoated substrate material, the mass change for CVD coated samples was decreased by 99.8%. This points to a significantly prolonged lifetime and shows the huge potential of coated Mo–9Si–8B alloys for application at very high temperatures and thermal cycling loads.
2. The influence of the cracks and pores induced by CVD coating on mechanical properties should be tested to get more insight into the properties of components and open the door to new applications.
3. The growth of the multilayer structure due to interdiffusion of CVD coatings shows an interesting and preferential behavior: The textural growth of the Mo_5Si_3 phase in [001]-direction leads to a low mismatch in thermal expansion coefficient between coating and substrate.

Acknowledgment

The authors kindly acknowledge the alloy supply by Plansee SE (Reutte, Austria). We also thank Mr. Philipp Watermeyer (DLR) for the EBSD measurement. JHP and TAS gratefully acknowledge the support of ONR (N00014-10-1-0913).

References

[1] J.H. Perepezko, Science 326 (2009) 1068–1069.
[2] G.W. Meetham, J. Mater. Sci. 26 (1991) 853–860.
[3] R. Darolia, Int. Mater. Rev. 58 (2013) 315–348.
[4] P. Jéhanno, M. Heilmaier, H. Kestler, Intermetallics 12 (2004) 1005–1009.
[5] P. Jéhanno, H. Kestler, A. Venskutonis, M. Böning, M. Heilmaier, B. Bewlay, M. Jackson, Metall. Mater. Trans. A 36 (2005) 515–523.
[6] M. Krüger, S. Franz, H. Saage, M. Heilmaier, J.H. Schneibel, P. Jéhanno, M. Böning, H. Kestler, Intermetallics 16 (2008) 933–941.
[7] J.A. Lemberg, R.O. Ritchie, Adv. Mater. 24 (2012) 3445–3480.
[8] M. Heilmaier, M. Krüger, H. Saage, J. Rösler, D. Mukherji, U. Glatzel, R. Völkl, R. Hüttner, G. Eggeler, Ch. Somsen, T. Depka, H. Christ, B. Gorr, S. Burk, JOM J. Miner. Met. Mater. Soc. 61 (2009) 61–67.

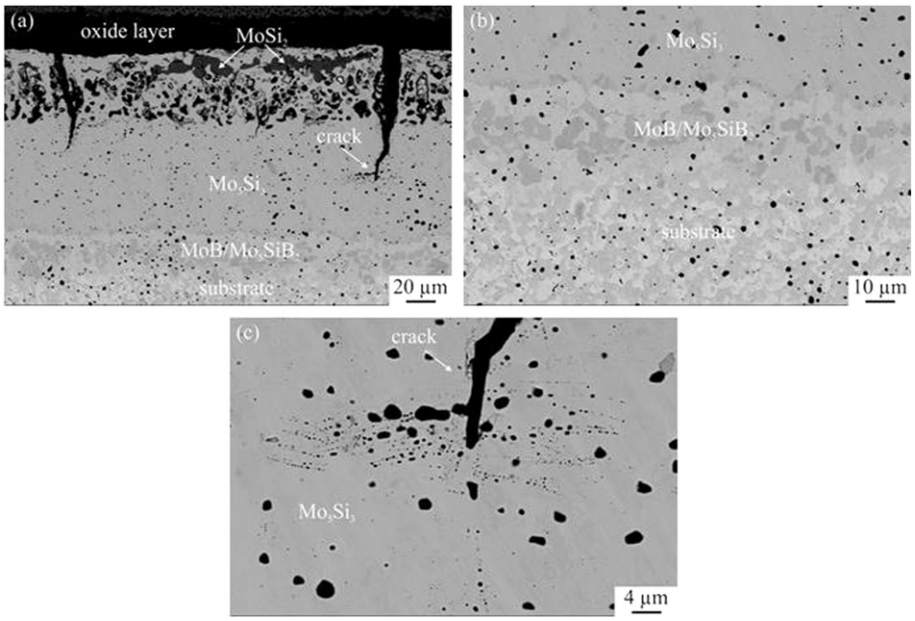

Fig. 10. (a) BSE-picture of the coated Mo–9Si–8B sample after oxidation at 1300 °C for 500 h, (b) image of the interlayer and (c) image of the crack tip.

[9] C. Hochmuth, D. Schliephake, R. Völkl, M. Heilmaier, U. Glatzel, Intermetallics 48 (2014) 3–9.
[10] S. Burk, B. Gorr, M. Krüger, M. Heilmaier, H.J. Christ, JOM J. Miner. Met. Mater. Soc. 63 (2011) 32–36.
[11] S. Majumdar, D. Schliephake, B. Gorr, H.J. Christ, M. Heilmaier, Metall. Mater. Trans. A 44 (2013) 2243–2257.
[12] I.P. Downs, J.H. Perepezko, R. Sakidja, S.R. Choi, Surf. Coat. Technol. 239 (2014) 138–146.
[13] O.J. Lu-Steffes, R. Sakidja, J. Bero, J.H. Perepezko, Surf. Coat. Technol. 207 (2012) 614–619.
[14] J.S. Park, R. Sakidja, J.H. Perepezko, Scr. Mater. 46 (2002) 765–770.
[15] J. Perepezko, R. Sakidja, JOM J. Miner. Met. Mater. Soc. 62 (2010) 13–19.
[16] J.H. Perepezko, R. Sakidja, JOM J. Miner. Met. Mater. Soc. 65 (2013) 307–317.
[17] P. Ritt, R. Sakidja, J.H. Perepezko, Surf. Coat. Technol. 206 (2012) 4166–4172.
[18] R. Sakidja, F. Rioult, J. Werner, J.H. Perepezko, Scr. Mater. 55 (2006) 903–906.
[19] A. Lange, R. Braun, Corros. Sci. 84 (2014) 74–84.
[20] A. Lange, R. Braun, M. Heilmaier, Intermetallics 48 (2014) 19–27.
[21] S. Kim, J.H. Perepezko, J. Phase Equilib. Diffus. 27 (2006) 605–613.
[22] R. Sakidja, J.H. Perepezko, Metall. Mater. Trans. A 36 (2005) 507–514.
[23] P. Jéhanno, M. Heilmaier, H. Saage, M. Böning, H. Kestler, J. Freudenberger, S. Drawin, Mater. Sci. Eng. A 463 (2007) 216–223.
[24] T.A. Kircher, E.L. Courtright, Mater. Sci. Eng. A155 (1992) 67–74.
[25] K. Yoshimi, S. Nakatani, T. Suda, S. Hanada, H. Habazaki, Intermetallics 7 (2002) 407–414.
[26] U. Helmersson, M. Lattemann, J. Bohlmark, A.P. Ehiasarian, J.T. Gudmundsson, Thin Solid Films 513 (2006) 1–24.
[27] R. Bandorf, V. Sittinger, G. Bräuer, in: S.H.F.B.J.V.T. Yilbas (Ed.), Comprehensive Materials Processing, Elsevier, Oxford, 2014, pp. 75–99.
[28] R. Bandorf, A. Bloche, K. Ortner, H. Lüthje, T. Jung, Plasma Process. Polym. 4 (2007) S129–S133.
[29] T. Jung, A. Westphal, Surf. Coat. Technol. 59 (1993) 171–176.
[30] H.L. Zhao, M.J. Kramer, M. Akinc, Intermetallics 12 (2004) 493–498.
[31] C.J. Rawn, J.H. Schneibel, C.M. Hoffmann, C.R. Hubbard, Intermetallics 9 (2001) 209–216.